LARGE-SCALE ACTIVITIES ASSOCIATED WITH THE 2003 OCTOBER 29 X10 FLARE

CHANG LIU, JEONGWOO LEE, NA DENG, DALE E. GARY, AND HAIMIN WANG

Center for Solar-Terrestrial Research
New Jersey Institute of Technology, University Heights, Newark, NJ 07102-1982

Submitted 2005 Sep.27; in revised form 2006 Jan.3 -- CL45@njit.edu

ABSTRACT

We present a multiwavelength study focusing on the large-scale activities associated with the 2003 October 29 X10 flare and a halo coronal mass ejection (CME). This event was so strong to clearly show several large-scale activities, such as, remote brightenings detected at Hα and soft X-rays, Moreton waves at Hα off-bands, and type II radio bursts, which offers an excellent opportunity to clarify the relationship among them. The remote brightenings were found near two coronal holes more than 2×10^5 km away from the main flare in eastern and southern directions, respectively. Coronal dimmings were seen at the locus of the remote brightenings right after the flare at both extreme-ultraviolet (EUV) and soft X-ray wavelengths. The Moreton waves propagated both northeastward and southward, toward the afore-mentioned remote regions, at speeds of approximately 1100 km s^{-1} and 1900 km s^{-1}, respectively. The type II radio bursts, while location and directivity are unidentified, are also observed to propagate at two different speeds. Our timing analyses show that the Moreton waves, the type II radio bursts, and the CME started almost simultaneously, but were not co-temporal with the remote brightenings. The remote brightenings are rather consistent, in timing and kinematics, with the flare hard X-ray emissions within the active region although they have much smaller scales. Based on these results, it is concluded that the two remote brightening regions were magnetically connected to the flaring active region, and that the remote brightenings as well as all other activities were due to the interaction of an erupting flux rope at the core of the flare with magnetic field overlying the region. The inferred scenario requires that the large overlying loops should open to allow the flare activity underneath them. In this sense, our results point to a picture similar to the magnetic break-out process in such a large scale.

Subject headings: Sun: activity — Sun: flares — shock waves — Sun: radio radiation — Sun: X-rays, gamma rays — Sun: coronal mass ejections (CMEs)

1. INTRODUCTION

Solar flares are local energy release phenomena in the scale of the flaring active region. It is however believed that even a larger scale magnetic field structure could be involved with the flare process, such as the scale of coronal mass ejection (CME). For this reason, it can be critically important to bring the local energy release into their global context in the solar atmosphere. An observational signature for the large-scale connectivity is remote brightening, radiation enhancement at Hα or soft X-rays found in regions distant from the flare site.

Remote brightening can be due to particles traveling from a flare core to the remote site along large-scale field lines. By studying two large flares in which Hα brightenings in remote quiet regions appeared simultaneously with reverse slope (RS) type III radio bursts, Tang & Moore (1982) suggested that the remote Hα brightenings were initiated by direct heating of the chromosphere by RS burst electrons traveling along discrete magnetic loops connecting the main flare to remote sites. Similar Hα phenomena with co-spatial microwave signature caused by fast electrons were also presented (Kundu et al. 1983; Nakajima et al. 1985; Hanaoka 1999). In this case, remote brightening can be an important tracer for a large-scale magnetic field connecting from the flare core to a distance place. Such a large loop itself is probably too tenuous to be directly observed, but is important in restructuring of magnetic fields as a result of, for instance, interaction between the erupting flare loop in the core region and the overlying large-scale magnetic fields. Subsequent formation of coronal holes (dimmings) were also found above the remote brightening regions (Manoharan et al. 1996). Since the dimming is often interpreted as representing the loss of the coronal mass swept into the CME, such a large-scale structure consisting of the main flare site and remote brightening is a good indicator of the onset of a CME.

Alternatively, remote brightenings can be initiated by disturbances propagating outwards from the flare site. The flare-associated globally traveling disturbances through the solar atmosphere have been detected by optical observations using Hα filtergrams by Moreton & Ramsey (1960). Uchida (1974a,b) argued that Moreton waves are a chromospheric manifestation of the flare-produced fast-mode MHD shocks propagating in the corona, which can also excite type II radio bursts. However, alternative driving mechanism of such shocks and the associated wave phenomena in the solar atmosphere has been proposed by Cliver et al. (2004). Moreton waves from explosive flares can cause progressive, short-lived distant brightenings of weak plages and elements of the chromospheric network as the expanding blast wave passes over them (Švestka 1976; Riegler et al. 1982). Rust & Webb (1977) suggested on the basis of their analysis of *Skylab* X-ray data that remote Hα brightenings can be caused by slow-mode shock waves seen in soft X-rays, which were further shown to be

consistent with the spread of thermal conduction fronts along coronal magnetic loops (Rust et al. 1985). In this case, remote brightening may not directly reveal a large-scale magnetic structure connected to the flare core, but still is important as an indicator of energy transport away from the flaring active region. Machado et al. (1988) concluded that all the three energy transport processes, namely, high-energy particles, shocks, and conduction fronts play significant roles in the redistribution of flare energy.

More recently, Balasubramaniam et al. (2005) reported a phenomenon called sequential chromospheric brightenings (SCBs) that are observed to propagate away from the flare site. They attribute the SCBs to the sequential tearing away of a series of nested magnetic loops during the eruption of a CME. This presents another challenge in understanding the nature of remote brightenings.

In this paper, we study the remote brightenings in Hα and soft X-rays together with Moreton waves, type II radio bursts, coronal dimmings, and CME that are observed during the 2003 October 29 X10 flare. Our main goal is to clarify the relationship among these activities, and eventually determine the large-scale magnetic structure. In §2, we describe the data used in this study. We present analyses of large-scale features in different wavelengths in §3 and a plausible reconnection scenario in §4. Major results are summarized in §5.

2. OBSERVATION

The 2003 October 29 flare was a very powerful, geo-effective event classified as 2B/X10.0. It occurred in the large superactive region NOAA 10486 (S15, W02), starting from 20:37 UT and reaching its maximum at 20:49 UT (*GOES* times). This event was well-covered by many space- and ground-based instruments. The images in Hα were taken with the Air Force *Improved Solar Observing Optical Network* (*ISOON*; Neidig et al. 1998). *ISOON* is an automated patrol telescope that uses a tunable Fabry-Pérot filter system to image the Sun in multiple wavelengths at rapid cadence. We used three full-disk images, in Hα center, Hα+0.4 Å, and Hα−0.4 Å. The time cadence of the images is 1 minute and the pixel resolution is $\sim 1''$ and $\sim 2''$ for the Hα center and off-bands, respectively. Remote brightenings were observed in each of these lines. However, due to the cloudy weather on that day, the Hα data could not be completely flat-fielded and the data quality was degraded[1]. Therefore, rather than following the usual approach of using the red wing images to probe the Moreton waves (e.g., Narukage et al. 2002), we made Hα Red−Blue wing subtraction images, which largely remove the image gradients. Our result shows that there were indeed Moreton waves

[1]Private communication with Nathan Dalrymple at National Solar Observatory.

propagating both northeastward and southward right after the flash phase of the flare. We note that the image times of H$\alpha-0.4$ Å and H$\alpha+0.4$ Å are $\sim$3 seconds apart during the observed time interval. This difference in the observed times was negligible in this study, because we only consider position difference in determining wave velocity.

Remote brightenings were also observed in soft X-rays with the *Solar X-ray Imager* (*SXI*; Hill et al. 2001) on board the *GOES* 12 satellite. The *SXI*'s 0.6–6.0 nm bandpass makes it sensitive to the coronal temperature range of 10^6–10^7 K. In this paper, we used images observed with the open filter position. The observing time cadence is about 4 minutes and the pixel resolution is $5''$.

Type II radio bursts associated with this event were recorded with the Culgoora Radiospectrograph (Prestage et al. 1994). The instrument operates over a frequency range from 18 MHz to 1.8 GHz and samples every three seconds. A CME was observed with the Large Angle and Spectrometric Coronagraph (LASCO; Brueckner et al. 1995) on board the *Solar and Heliospheric Observatory* (*SOHO*; Domingo et al. 1995) and we used the CME height-time data that are provided by the LASCO Web site. Large-scale coronal dimmings are seen for this event in extreme-ultraviolet (EUV) images that were observed with the EUV Imaging Telescope (EIT; Delaboudinière et al. 1995) on board *SOHO*. The observation in this study was made in a wavelength range centered on 195 Å, comprising an Fe XII line emitted at 1.2×10^6 K at typical coronal density. The EIT pixel resolution is $2.6''$.

In order to explore the dynamics in the flare core region and understand the relation between the large-scale activities and energy release sites, we used hard X-ray light curves and images from the *Reuven Ramaty High Energy Solar Spectroscopic Imager* (*RHESSI*; Lin et al. 2002). We also obtained microwave emissions at 1.2–18.0 GHz from coordinated Owens Valley Solar Array (OVSA; Gary & Hurford 1990) observations to investigate the nonthermal properties of this event.

The magnetic field and white-light structure of the photosphere were observed with the Michelson Doppler Imager (MDI; Scherrer et al. 1995) on board *SOHO*. For the data used in the current study, the cadence was 96 minutes and 6 hours for the magnetic and white-light data, respectively, with an image scale of $2''$. We also used the soft X-ray light curve observed by *GOES* satellite to track the timing of this flare.

3. DATA ANALYSIS

3.1. Remote Brightenings in Hα and SXR

The very complicated active region NOAA 10486 was about 15° south of the equator and was just west of central meridian on 2003 October 29. Figures 1*a* and 1*b* show the two extended remote brightenings (denoted as "RHBs") observed in Hα that lay east and south of the X10 flare core (denoted as "F"), respectively. Note that these two remote brightenings occurred at different times and exhibited different morphology. The arrows in Figure 1*a* point to the eastern remote brightening chain in the shape of a letter L, which comprises several discrete brightened patches with the earliest onset time at ∼20:41 UT. The brightening chain is more than 2×10^5 km away from the main flare site. Figure 1*b* shows the initial position of the southern remote brightening which is more than 3×10^5 km away from the flare core and was initiated at ∼20:49 UT. The brightening site was then observed to move southeast toward the limb. To better show the weak magnetic field outside the active region especially near the polar area, we used 20-minute average around 20:49 UT on the MDI magnetograms and presented the result in Figure 1*c*. It is obvious that the eastern remote brightening patches lie in the negative polarity region. For the southern remote brightening site that is near the south pole, the polarity is generally positive with many magnetic kernels clearly to be seen. From the EIT 195 Å image shown in Figure 1*d*, we can see that both the eastern and southern remote brightenings are located in the vicinity of coronal holes (CH). Since the magnetic field lines outside the coronal holes return to the surface, we deduce that the remote brightenings are the footpoints of large-scale closed loops.

Figure 2 shows the evolution of the L-shaped eastern remote brightening in Hα. The remote bright chain first brightened in the end furthest away from the flare core (patches 1–4), then in the near ends (patches 5–7). At ∼20:44 UT, more than ten individually brightened patches can be seen. The time between onset and maximum brightness of the major kernels 1–4 is about 6 minutes. For the southern remote brightening shown in Figure 3, there are two brightening branches as indicated by letter *a* and *b* at 20:49 UT, respectively. The latter branch gradually faded away after about 4 minutes, while the former one propagated southeast toward limb with successively activated bright patches (*c*–*f*).

Similar remote brightenings were also observed in soft X-rays. A time-lapse *SXI* movie shows that the southern remote brightening moved southeast toward the limb, identical to the motion observed in Hα. One frame at ∼20:53 UT is presented in the right panel in Figure 4. However, due to the lack of time resolution, there is only one frame that is at ∼20:45 UT showing the eastern remote brightening (left panel in Fig. 4), but with almost the same morphology as seen in Hα (see Fig. 1*a*).

We compared the present remote brightenings with the SCBs reported by Balasubramaniam et al. (2005). They are similar in that small chromospheric features outside the flare core brightened in both events. Differences lie in their morphology. First, the SCBs successively brightened with distance from the flare, while the two extended remote brightening sites presented in this study were found more than 2×10^5 km away from the main flare with neighboring coronal holes. Second, the SCBs were initiated following an eruption, while the two remote brightenings in our event have different timings and are associated with the two main stages of flare energy release, respectively (see §3.3 below).

3.2. Moreton Waves and Type II Radio Bursts

We traced the Moreton waves by difference images of *ISOON* Hα off-bands. Figure 5 shows the full-disk images of this event in Hα off-bands subtraction and EIT 195 Å with the overplotted locations of the wave fronts (*solid lines*), which were determined visually using the subtraction images. The northern Moreton wave first propagated northeastward, then changed its direction toward northwest, probably because it encountered the coronal hole region there ("CH", also see Fig. 1*d*). The southern Moreton wave propagated all the way to the south pole. The dashed lines are the paths of the Moreton waves, which are drawn as parts of great circles on solar surface taking into account the curvature of the Sun. Along each path, we measured the photospheric distances of the fronts from the supposed origins that were determined considering the shape of the wave fronts and the evolution of the Hα flare. Oscillations of several quiescent filaments in the northern hemisphere (*arrows* in Fig. 5*a*) were also observed at about 20:53 UT, which indicates that the northern Moreton wave passed by them.

The type II radio bursts associated with this event are identified on the Culgoora radiospectrograph shown in Figure 6. The metric type II bursts began at ∼20:42 UT with starting frequency ∼400 MHz and ended at ∼20:50 UT at ∼60 MHz. The fundamental and harmonic emissions are marked with dotted and dashed lines, respectively. Both components appear in two branches. The first branch drifted very fast till ∼20:43 UT, while the second branch drifted more slowly, lasting for about 5 minutes. To determine the speed of type II radio bursts, we convert the frequency drift seen in the spectrograph to distance from the photosphere under a coronal electron density model. Such conversion depends on the model and we choose the one proposed by Newkirk (1961) as it has been shown to better represent the inner corona (e.g., Warmuth & Mann 2005). Using this admittedly rough approximation, the extrapolated speeds of the two branches of type II radio bursts are found to be ∼2000 and ∼900 km s^{-1}, respectively, with almost the same start time at ∼20:42 UT.

The time/distance diagram for the Morton waves, the type II radio bursts, and the CME are shown in Figure 7, together with overplotted lightcurves of *GOES* soft X-ray flux at the 1–8 Å channel and *RHESSI* 50–100 keV photons for comparison. The distances of the Moreton wave fronts are measured from the flare site along the great circles (See Fig. 5). It is obvious that the southern and northeastern traveling Moreton waves are spatially correlated with the faster and slower branches of the type II radio bursts, respectively, with similar speeds (at ∼1900 and ∼1100 km s^{-1}, respectively) and start times (∼20:42 UT), suggesting that these two phenomena are closely related. It is also interesting to point out that the northeastern traveling Moreton wave was "reflected" by the coronal hole region at ∼20:46 UT with subsequently reduced speed at ∼760 km s^{-1}. The corresponding type II radio bursts was slightly slowed down to ∼800 km s^{-1}. We thus infer from these results that the Morton waves and the type II radio bursts are simultaneous with each other. On the other hand, Figure 7 shows that the timing of remote brightenings (denoted by *asterisks*) do not correlate with the Moreton waves. It is thus unlikely that the Moreton waves are the trigger of the remote brightenings.

The EIT wave is another wave-like phenomenon in the solar corona (Thompson et al. 1998, 1999) and we show in Figure 8 the running differences of EIT images before and after the eruption. The detection of an EIT wave in these data is difficult because of the widespread emission (extended bright region) seen in Figure 8*b*, either characterized as a "global enhancement" or attributed to instrumental scattered light (Cliver et al. 2004, and references therein). We thus found no clear signature of an EIT wave in this event. However, we will discuss the dimming regions seen in Figure 8*b,c* in §3.4.

3.3. Timing of the Flare Emissions

In Figure 9, we plot flare emissions at hard X-ray, microwave, and radio wavelengths in terms of their dynamic spectra. For comparison, we also overplot the time profiles of flux of the major Hα remote brightening kernels (middle panel). All the dynamic spectra show that the flare consists of two major peaks: the first peak lying from about 20:40 UT to 20:49 UT and the second from about 20:49 UT to 21:00 UT. Note that the eastern remote brightening (white circles) coincides with the first phase of the flare, and the southern remote brightening (grey circles), with the second phase. The overplotted lightcurve (black line) of the western hard X-ray sources (see Fig. 11) further shows that the onset time of the major eastern remote Hα brightening kennels 1-4 at 20:41 UT (first vertical dashed line) coincides with the first spike in hard X-ray and microwave. The peak times of eastern remote brightening kernels are also correlated with the peak emissions in hard X-ray and microwave. Similar

correlation is found for the southern remote brightening.

Therefore, the remote brightenings are rather well-related to the flare core emissions. This finding suggests that the remote brightenings may be due to direct chromospheric heating by the flare-accelerated electrons traveling along the large-scale magnetic loops connecting the flare core to the remote patches. Furthermore, the remote brightenings in the eastern and southern sites are associated with the first and second energy release process in the main flare, respectively.

The two phases shown in the radiospectrograph (bottom panel) are clearly characterized by the type II emissions and the radio pulsations (indicated by arrows), respectively. Since the radio pulsations can be regarded as a signature of dynamic magnetic reconnection (e.g., Kliem et al. 2000), the finding of association of type II emissions and radio pulsations with two distinct flaring phases bolster our argument of this eruption as two different processes (see discussions in §4 below). Detailed study of the radio pulsation structure is beyond the scope of this paper.

3.4. Coronal Dimming and CME

We found coronal dimmings associated with this event in both EIT and *SXI* images. The top row of Figure 10 shows EIT 195 Å images before the flare (19:39 UT) and after the flare (21:48 UT) and the difference between two. The middle row shows preflare and postflare and the difference between the *SXI* images. Note that we choose the soft X-ray image about 3 hours after the flare as postflare image in order to avoid the scattered light in the telescope right after the flash phase of the flare (see Fig. 4). Care was also taken to differentially rotate all frames to 20:30 UT before subtraction. Two very similar dimming regions in EUV and soft X-ray are found and marked by "A" and "B" in the difference images. It is clearly visible that the two coronal dimmings are well associated with the two remote Hα brightenings, respectively, shown in the bottom middle and right panels. The bottom left panel shows a MDI magnetogram at 20:30 UT for comparison and it can be seen that the two Hα remote brightenings are located in opposite polarity magnetic fields. Based on Figures 8 and 10, we note the following. First, Figure 8*b,c* shows that the eastern *A* and southern *B* dimming regions formed at different times, approximately following the occurrence of eastern and southern remote brightenings, respectively. The fact that the dimmings occurred at two different times supports our previous conclusion that two distinct energy release processes were involved with this eruption and each caused large-scale disturbances in the solar atmosphere. Second, the locus of these dimming regions are well aligned with those of the remote brightenings, suggesting that the remote brightenings

occurred in the regions that eventually became evacuated to form extensions of the pre-existing coronal holes that they border. Since dimmings are considered as due to the loss of the coronal mass swept into CMEs along open field lines (e.g., Pohjolainen et al. 2005), the coronal dimmings found associated with the remote brightenings in this event may imply the opening of large-scale magnetic loops that were linking the remote brightening regions to the flare core as deduced in §3.3.

A halo CME associated with this event was observed. It was first seen in C2 at 20:54:05 UT as a bright loop front over the south pole extending to $\sim$2.9 $R_\odot$. We used the CME height-time data provided by the LASCO Web site to find the average speed of the leading edge to be about 2029 km s^{-1}. This speed is very similar to that of the faster branch of the type II radio burst and the southern traveling Moreton wave, implying their common origin. We also extrapolated the height-time data back to the flare site assuming a constant deceleration to find the CME starting at $\sim$20:42 UT (see Fig. 7), which is very close to the onsets of Moreton waves and the type II radio bursts. We can thus conclude that the the Moreton waves, the type II radio bursts, and the CME are concurrent in this event. Close timing of Moreton wave, type II radio burst, and CME was also reported by Eto et al. (2002).

3.5. Flare Footpoint Motions

We show, in Figure 11, the *RHESSI* 50–100 keV hard X-ray source motions overplotted onto the MDI magnetogram. The kinematic morphology of the hard X-ray footpoints can be categorized into two phases. First, before about 20:49 UT, the hard X-ray emission is very complex and the footpoint motion is not clear. Two separate sources are seen in the western side at the beginning, while the source labeled W2 disappeared around 20:43 UT. As we discussed in §3.1 and §3.3, the remote brightening kernels 1-4 lie further away from the flare core but brightened earlier than those closer ones. A similar disjointed time-distance sequence of remote brightenings was also reported by Tang & Moore (1982). The eastern remote brightening kernels are also temporally associated with the western hard X-ray sources. These facts actually rule out the possibility of a shock wave propagating away from the flare site as the exciting agent of remote brightening, while favoring direct heating of the chromosphere by hot electrons traveling along large-scale loops. Second, the standard motion of hard X-ray footpoints as well as ribbons seen in Hα and UV wavelengths, i.e., separating away from the magnetic neutral line, is clearly seen during the second energy release process of the flare after about 20:49 UT. The eastern hard X-ray source moves obviously about 25″ toward the east, and the western source about 15″ toward the west. Interestingly, the

southern remote brightening kernels also exhibit motion toward the east (see §3.1), the same direction and during the same period as the eastern hard X-ray source. We therefore presume that the small-scale motion (less than 50″) of flare footpoints in the core region could represent a "mapping" of the large-scale restructuring, manifested as remote brightenings.

We thus believe that the hard X-ray footpoint motions showing distinct behaviors in two phases is an important clue to the 3D magnetic reconnection. According to the standard 2D reconnection model (Priest & Forbes 2002), the progressive footpoint motion indicates magnetic reconnection in the coronal X-point. In the first stage (before ∼20:49 UT), however, we do not see such systematic hard X-ray footpoint motion, probably owing to the 3D structure of the large-scale magnetic field that is not taken into account by the model. It is in the second stage (after ∼20:49 UT) that we could see the progressive footpoint separation as predicted by the standard model. Krucker et al. (2005) carried out a detailed analysis of this footpoint motion to find a good correlation between the electron energy and the magnetic energy release in the second stage. It therefore implies that the 3D magnetic field evolves into a configuration resembling the standard 2D reconnection model, perhaps as a result of the large-scale loop interaction in the first stage.

4. Speculation on the Large-scale Magnetic Fields

Since our analysis suggests the presence of large-scale magnetic connections, we consider it appropriate to specify such a magnetic structure and its evolution during the flare. Our speculation here is mainly based on the magnetic polarity. In Figure 12*a*, we plot the magnetic field configuration in the preflare state. The eastern remote brightening region has negative magnetic polarity and it should be connected to the positive polarity in the flare active region (black line). The southern remote brightening region has positive polarity and therefore connects to the negative polarity of the flare core (white line). Finally, the connectivity around the neutral line inside the active region (gray line) can be assumed. Under this configuration, it is the gray and black lines that can, upon interaction, lead to the first phase of the flare emissions and the remote brightening in the east altogether.

The second phase is characterized by the hard X-ray footpoint as well as Hα/UV ribbon separation from the magnetic neutral line and the southern remote brightening. As discussed in §3.5, this progressive motion could fit into the standard reconnection model. Figure 12*b* shows such magnetic configuration. As the reconnection point rises higher, the footpoints move further away from the magnetic neutral line. Some portion of the hot particles precipitating along the recently reconnected field lines (thick gray line) can also drift to the ambient field lines that are connected to the southern remote brightening region (i.e., transported

from the thick gray line to the white line; Lau & Ramaty 1995). As a result, the southern brightening occurred during the second phase of the flare.

The pre- and postflare configurations shown in Figure 12*a,b* may explain the flare activities associated with the first and the second phase, respectively. One issue, however, is that the magnetic evolution from the preflare to the postflare state requires that the overlying field (black line) should open, which becomes CME, in order to allow the inner loop system (gray line) to grow outward. This opening can be realized by reconnection of the black line and the gray line, but whether or not such reconnection is physically possible becomes another issue. Although this question is beyond the scope of this study, we report some characteristics in the long-term evolution of this active region that could be related to the triggering of such reconnection. First, we found that magnetic flux emergence occurred in the flaring part of the active region (gray line). Examination of the MDI magnetograms from October 28 to 31 shows that the positive and negative flux within the region P and N increased by about 1.9 $\times 10^{21}$ and 0.7 $\times 10^{21}$ Mx, respectively (Fig. 12*c*). Our previous study also reveals that the magnetic shear along the flaring neutral line increased after this event (Liu et al. 2005). We interpret the apparent shear increase as due to emergence of sheared magnetic fields, which can help to trigger the reconnection of the active region fields (gray line) with the overlying fields (black line) (Feynman & Martin 1995). Second, the evolution in MDI white-light (Fig. 12*d,e*) shows that the spots F1 and F2 had counterclockwise rotation by about 180° during about 4 days period before the flare. Such rotation of sunspot will twist the active region fields (gray line), making them more prone to erupt (Sturrock et al. 2001). The twisted field lines can also have a larger tilt angle with respect to the overlying field to enhance the probability of reconnection. Finally, the reconnection in such a case will occur in a way to unwind the magnetic twist, i.e., reverse the rotation. We may then expect that the Moreton waves and the type II radio bursts would be generated with a wide directivity toward the east and south regions, in agreement with the above observation (see Fig. 5).

5. SUMMARY

In this paper, we have studied the large-scale activities associated with the 2003 October 29 flare. The initial motivation of this study was the mechanism for the remote brightenings associated with this flare, but it also led us to the study of the relationship between CME, Moreton waves, and type II bursts. Our results can be summarized as follows:

1. We have checked the timing of the Hα remote brightenings against the Moreton waves and the type II radio bursts. In our result, the Moreton waves and the type II radio

bursts are simultaneous, but do not coincide with the remote brightenings and thus they cannot be the trigger mechanism for the remote brightenings in this event.

2. The remote brightenings are closely related to the flare core emissions in time and morphology. We therefore consider that the direct heating by hot particles transported along closed magnetic fields is more appealing as the mechanism for the remote brightenings. This result suggests the presence of large-scale connections between the remote brightenings and the flare core.

3. Our timing analysis revealed that the CME, the Moreton waves, and the type II radio bursts could have occurred simultaneously. This may suggest that CME could be a viable driver for the Moreton waves as well as type II radio bursts (Cliver et al. 2004).

4. The magnetic reconnection has to occur in two distinct stages in order to explain both lightcurves and morphological changes in the flare core and the remote brightening regions. In the first stage, a flux rope in the active region interacts with the overlying field to cause the first flare emission phase and the eastern remote brightening. In the second stage, the flux rope erupts and reconnects to cause continuous hard X-ray footpoints separation and the southern remote brightening.

5. Coronal dimmings were found at the locus of the two remote brightening regions, respectively. We take this as another piece of evidence for the idea that this remote brightenings are due to magnetic reconnection rather than traveling disturbances.

6. From the long-term evolution of the active region, we suggest that the emergence of sheared magnetic fields and the accumulation of magnetic twist due to sunspot rotation could trigger the first stage reconnection, which is responsible for most of the large-scale activities including the Moreton waves, type II radio bursts, CME, the eastern remote brightening, as well as the flare core emissions.

In the sense that our inferred scenario requires a removal of overlying field to allow the flare activity underneath, it favors a reconnection picture analogous to the magnetic breakout model (Antiochos 1998; Antiochos et al. 1999). A distinctive feature of this event is however that the two types of reconnection, one leading to the removal of the overlying field and the other associated with the flare ribbon motion, are well separated in time perhaps owing to the large dimension of its magnetic configuration. We thus propose that the remote brightenings and the flare emissions in this event could be a good example for clarifying the CME and flare processes in the magnetic break-out model.

The authors thank *ISOON*, Culgoora, *RHESSI*, *SOHO*, and OVSA teams for providing excellent data sets. We are especially grateful to Nathan Dalrymple at National Solar Observatory and Nigel Prestage at Culgoora Solar Observatory to make the Hα and radio data, respectively, available to us. We thank the referee for valuable remarks and suggestions that resulted in improvement of the paper. C. L. also thanks J. Qiu and V. Yurchyshyn for helpful discussions. *ISOON* project is a collaboration between the Air Force Research Laboratory Space Vehicles Directorate and the National Solar Observatory. Culgoora Solar Observatory is part of IPS, which is a unit of the Australian Government Department of Administrative Services. *RHESSI* is a NASA Small Explorer. *SOHO* is an international collaboration between NASA and ESA. This work is supported by NASA under grants NAG5-13661 and NNG0-4GG21G and by NSF under grant ATM-0313591. The OVSA is supported by NSF grant AST-0307670 to New Jersey Institute of Technology.

REFERENCES

Antiochos, S. K. 1998, ApJ, 502, L181

Antiochos, S. K., Devore, C. R., & Klimchuk, J. A. 1999, ApJ, 510, 485

Balasubramaniam, K. S., et al. 2005, ApJ, 630, 1160

Brueckner, G. E., et al. 1995, Sol. Phys., 162, 357

Cliver, E. W., Nitta, N. V., Thompson, B. J., & Zhang, J. 2004, Sol. Phys., 225, 105

Delaboudinière, J.-P., et al. 1995, Sol. Phys., 162, 291

Domingo, V., Fleck, B., & Poland, A. I. 1995, Sol. Phys., 162, 1

Eto, S., et al. 2002, PASJ, 54, 481

Feynman, J., & Martin, S. F. 1995, J. Geophys. Res., 100, 3355

Gary, D. E., & Hurford, G. J. 1990, ApJ, 361, 290

Hanaoka, Y. 1999, PASJ, 51, 483

Hill, S. M., Pizzo, V. J., Wilkinson, D. C., & Davis, J. M. 2001, AGU Spring Meeting (Washington, DC: AGU), 61, 6

Kliem, B., Karlický, M., & Benz, A. O. 2000, A&A, 360, 715

Krucker, S., Fivian, M. D., & Lin, R. P. 2005, Adv. Space Res, 35, 1707

Kundu, M. R., Rust, D. M., & Bobrowsky, M. 1983, ApJ, 265, 1084

Lau, Y.-T. & Ramaty, R. 1995, Sol. Phys., 160, 343

Lin, R. P., et al. 2002, Sol. Phys., 210, 3

Liu, C., Deng, N., Liu, Y., Falconer, D., Goode, P. R., Denker, C., & Wang, H. 2005, ApJ, 622, 722

Machado, M. E., Xiao, Y. C., Wu, S. T., Prokakis, Th., & Dialetis, D. 1988, ApJ, 326, 451

Manoharan, P. K., van Driel-Gesztelyi, L., Pick, M., & Démoulin, P. 1996, ApJ, 468, L73

Moreton, G. E., & Ramsey, H. E. 1960, PASP, 72, 357

Nakajima, H., Dennis, B. R., Hoyng, P., Nelson, G., Kosugi, T., & Kai, K. 1985, ApJ, 288, 806

Narukage, N., Hudson, H. S., Morimoto, T., Akiyama, S., Kitai, R., Kurokawa, H., & Shibata, K. 2002, ApJ, 572, L109

Neidig, D. et al. 1998, in Synoptic Solar Physics, ASP Conf. Ser. 140, ed. K. S. Balasubramaniam, J. Harvey, & D. Rabin, 519

Newkirk, G. Jr. 1961, ApJ, 133, 983

Pohjolainen, S., Vilmer, N., Khan, J. I., & Hillaris, A. E. 2005, A&A, 434, 329

Prestage, N. P., Luckhurst, R. G., Paterson, B. R., Bevins, C. S., & Yuile, C. G. 1994, Sol. Phys., 150, 393

Priest, E. R., & Forbes, T. G. 2002, A&A Rev., 10, 313

Riegler, G. R., et al. 1982, ApJ, 259, 392

Rust, D. M. & Webb, D. F. 1977, Sol. Phys., 54, 403

Rust, D. M., Simnett, G. M., & Smith, D. F. 1985, ApJ, 288, 401

Scherrer, P. H., et al. 1995, Sol. Phys., 162, 129

Sturrock, P. A., Weber, M., Wheatland, M. S., & Wolfson, R. 2001, ApJ, 548, 492

Švestka, Z. 1976, Solar Flares (Dordrecht: Reidel)

Tang, F., & Moore, R. L. 1982, Sol. Phys., 77, 263

Thompson, B. J., Plunkett, S. P., Gurman, J. B., Newmark, J. S., St. Cyr, O. C., & Michels, D. J. 1998, Geophys. Res. Lett., 25, 2465

Thompson, B. J., et al. 1999, ApJ, 517, L151

Uchida, Y. 1974a, in IAU Symp. 57, Coronal Disturbances, ed. G. Newkirk (Dordrecht: Reidel), 383

Uchida, Y. 1974b, Sol. Phys., 39, 431

Warmuth, A., & Mann, G. 2005, A&A, 435, 1123

This preprint was prepared with the AAS LaTeX macros v5.2.

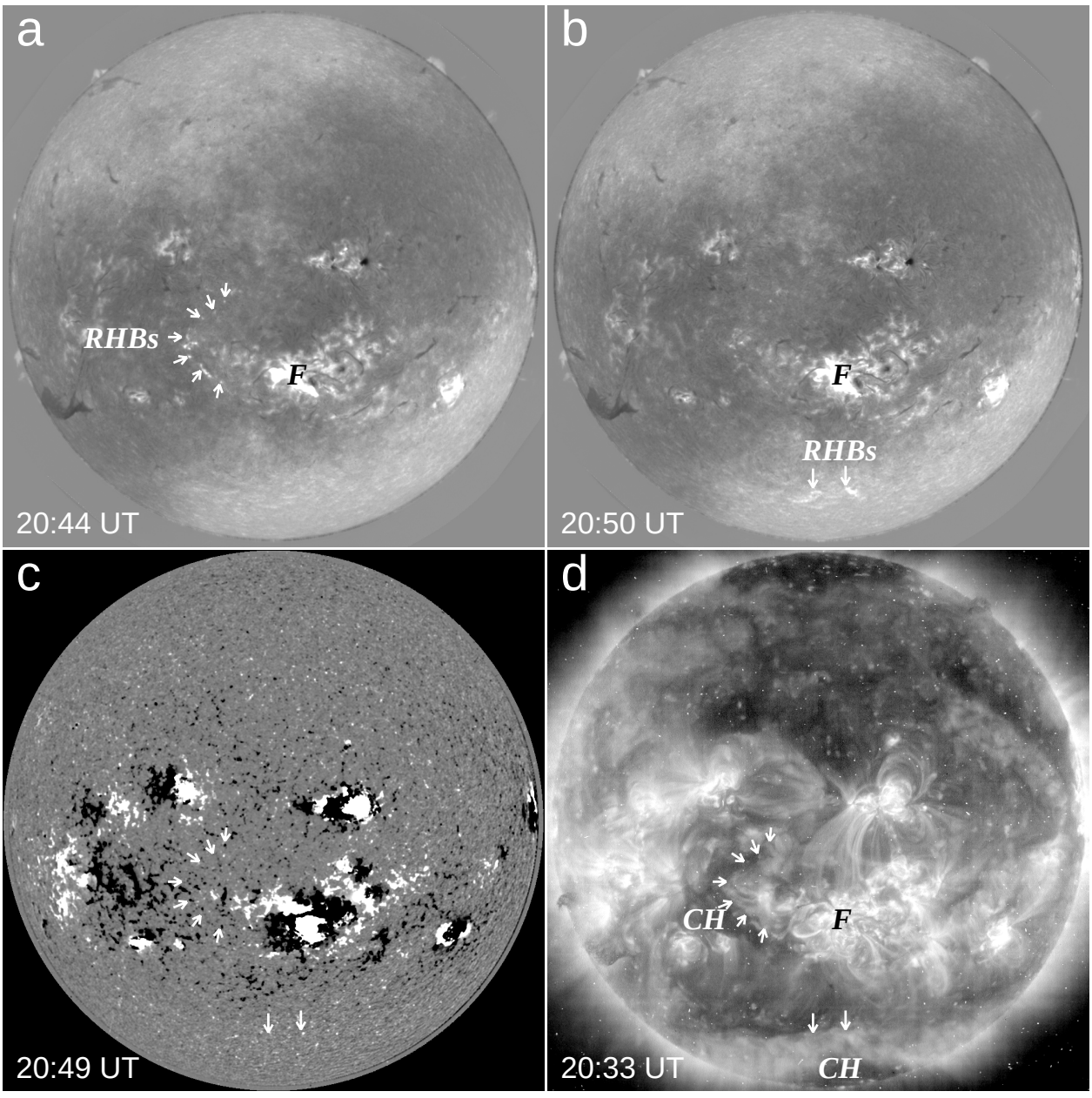

Fig. 1.— (*a* and *b*) Hα images from *ISOON* showing the two extended remote Hα brightenings (RHBs; denoted by arrows) that started at different times, as well as the flare core (denoted as "F"). The eastern remote brightening (panel *a*) is in the shape of a letter L and the southern remote brightening (panel *b*) propagated southeast toward limb. (*c*) 20-minute averaged MDI magnetogram centered at 20:49 UT. (*d*) EIT 195 Å image showing the two coronal holes (CH) near the remote brightenings.

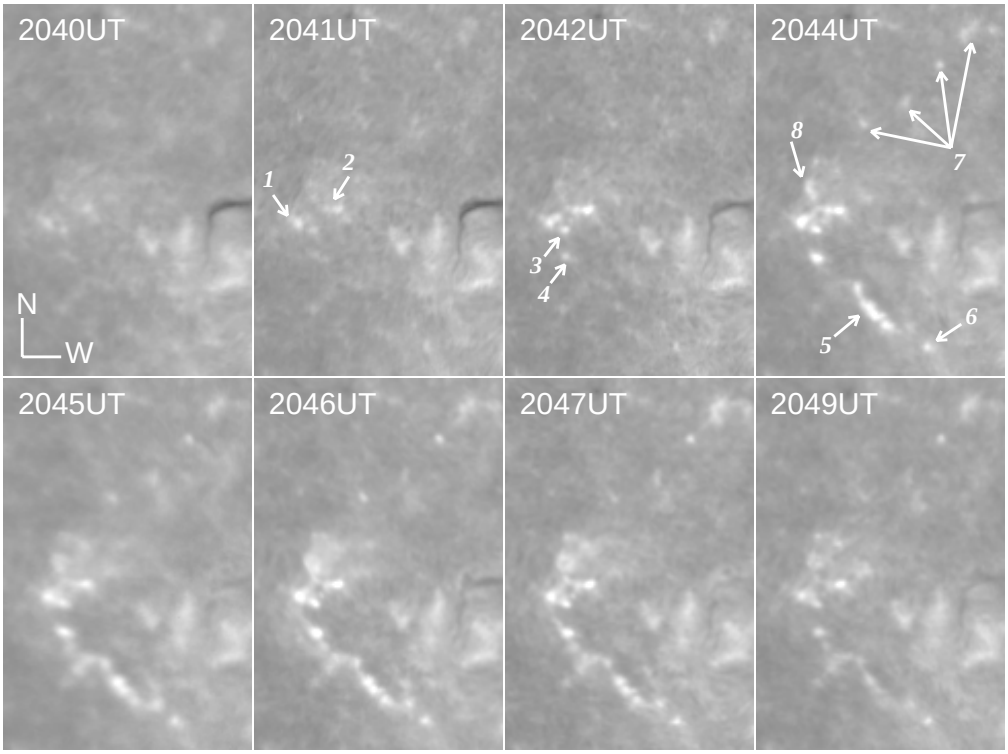

Fig. 2.— Time sequence of *ISOON* Hα images showing the dynamics of eastern remote brightening chain denoted in Figure 1*a*. Arrows with corresponding numbers indicate individual new brightening kernels as they began to glow. The field of view is 260″× 390″.

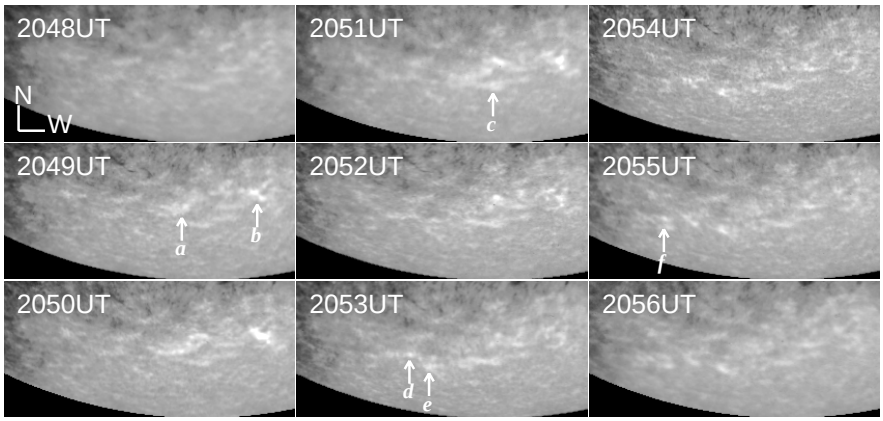

Fig. 3.— Time sequence of *ISOON* Hα images showing the dynamics of southern remote brightening that propagated southeast with its initial position indicated in Figure 1*b*. Arrows with corresponding letters indicate individual new brightening kernels as they began to glow. The field of view is 610″× 280″.

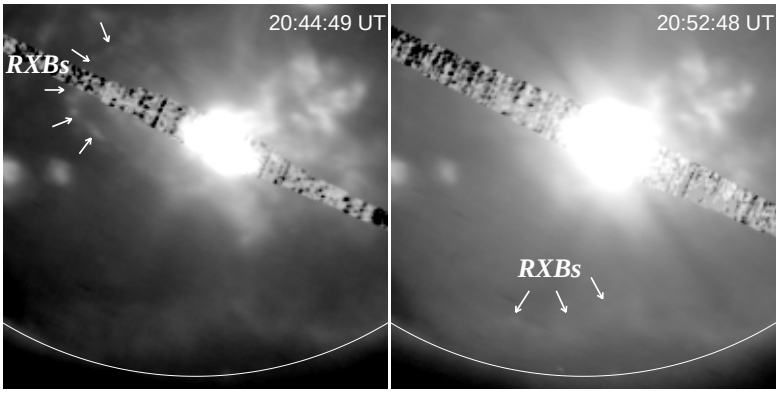

Fig. 4.— Soft X-ray images from *SXI* using the open filter position. The left panel at ∼20:45 UT shows the eastern remote soft X-ray brightenings (RXBs) in the shape of a letter L (denoted by arrows). The right panel at ∼20:53 UT shows the position of the southern remote brightening patches similar to those seen in Hα. The white line represents the solar limb. The field of view is 1000″× 1000″. West is to the right, and solar north is up.

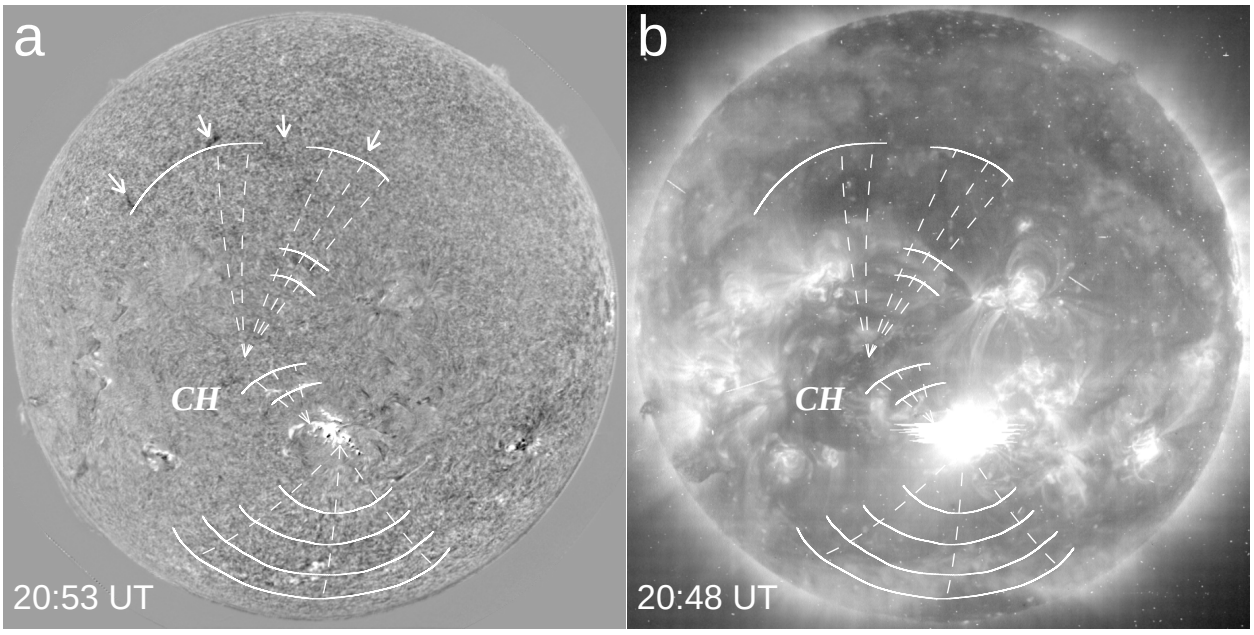

Fig. 5.— Hα Red−Blue subtraction (a) and EIT 195 Å (b) images. Overplotted are wave fronts (*solid lines*) and parts of great circles (*dashed lines*) along which the distances from the supposed origin of the Moreton waves were measured. Times (in UT) for the northern traveling wave fronts are 20:43, 20:44, 20:46, 20:47, and 20:53. For the southern traveling wave fronts, they are 20:43, 20:44, 20:45, and 20:46. The locations of the filaments that started to oscillate when the Moreton wave past over them are indicated by arrows. "CH" indicates the coronal hole region.

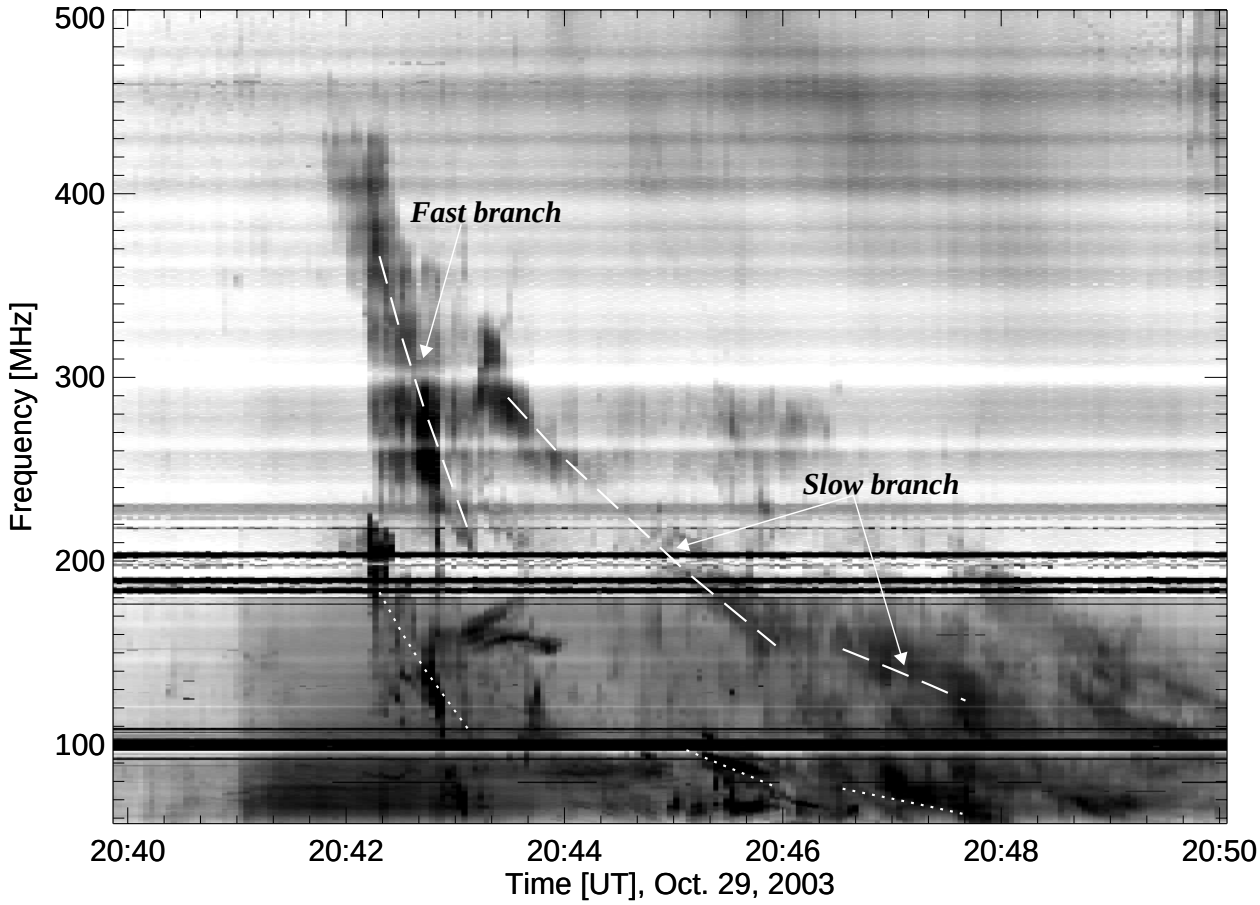

Fig. 6.— Radio data for about 20:40–20:50 UT on 2003 October 29 observed with the Culgoora Radiospectrograph, showing the type II radio bursts from ∼20:42–20:50 UT. *Dotted* and *dashed* lines depict the fundamental and harmonic components of the type II emissions, respectively.

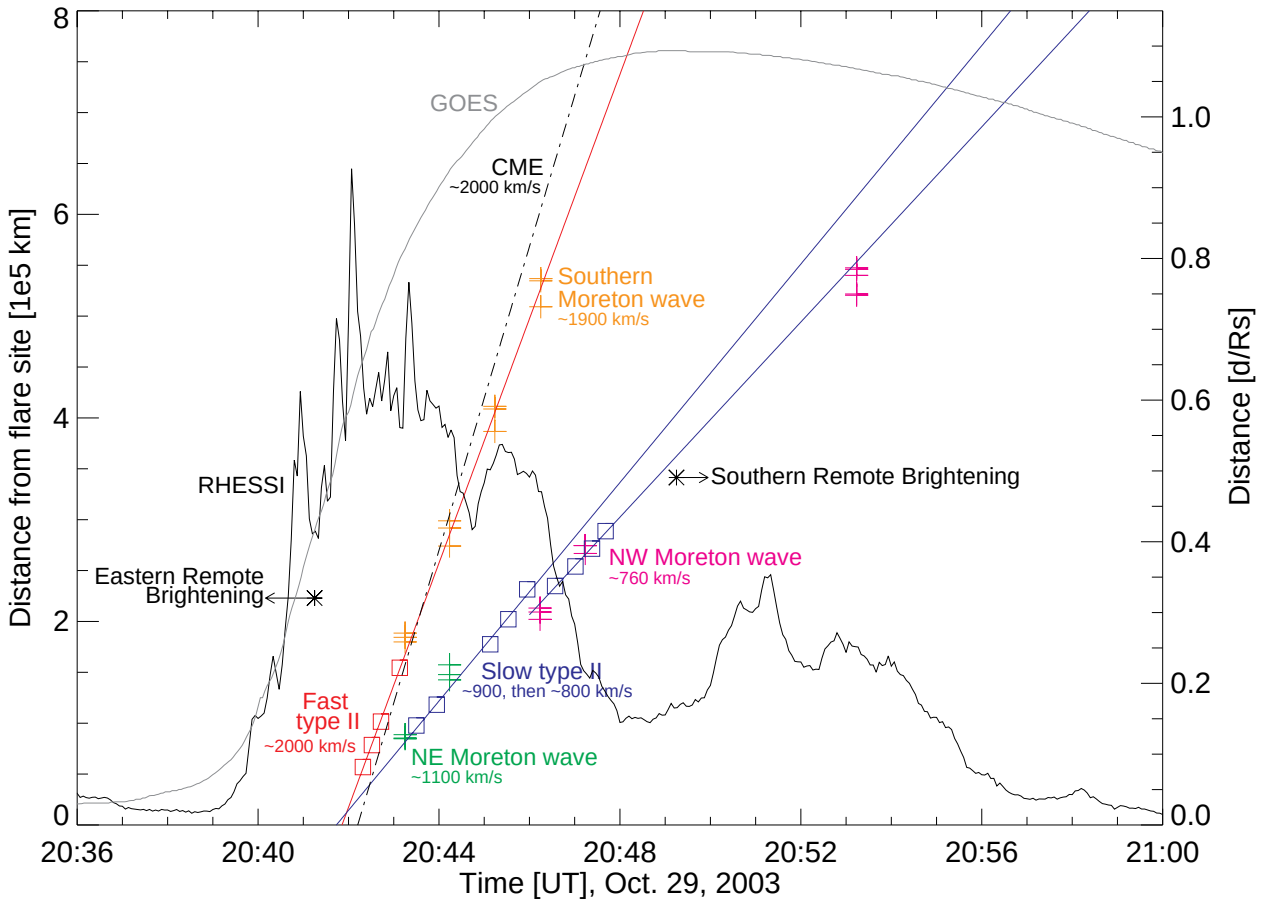

Fig. 7.— Time evolutions of the distances of the type II radio bursts, the Moreton waves, and the CME, overplotted with *GOES* 10 soft X-ray flux at the 1–8 Å channel and *RHESSI* 50–100 keV photons binned into 4 s intervals. The vertical axis represents the distances from the flare site along the great circles (see Fig. 5) for the Moreton waves, the distances from the photosphere calculated with the Newkirk's coronal electron density model for the type II radio bursts, and the height of the CME by extrapolating a constant deceleration fit back to the flare site. Note that the CME leading edge was at 2.92 $R_\odot$ at the time of the first LASCO image at 20:54:05 UT. *Asterisks* denote the earliest onset time and corresponding distances from the flare site of remote brightenings. "Rs" represents the solar radius (695,800 km).

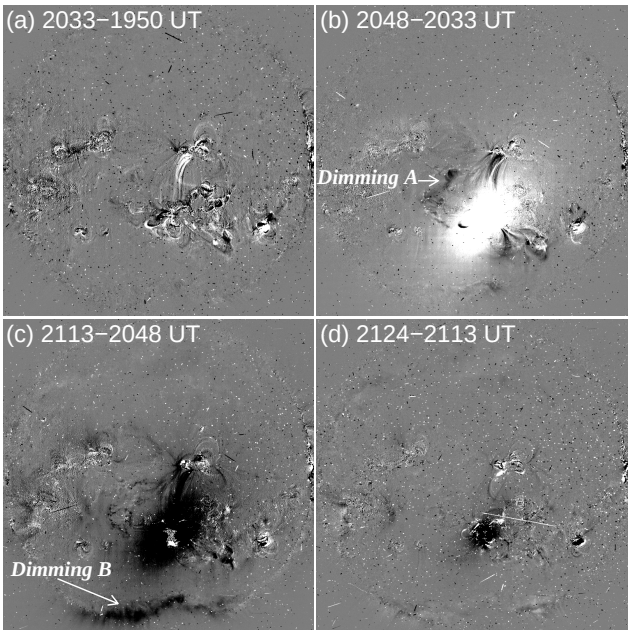

Fig. 8.— *SOHO*/EIT 195 Å running-difference images. The sequence consists of EIT 195 Å images at (*a*) 20:33 UT, (*b*) 20:48 UT, (*c*) 21:13 UT, (*d*) 21:24 UT, with previous images subtracted from them. Widespread emission is seen in (*b*) as an oval structure. The coronal dimming regions *A* and *B* indicated by the arrows in (*b*) and (*c*), respectively, are also outlined in Fig. 10 (see discussions in §3.4).

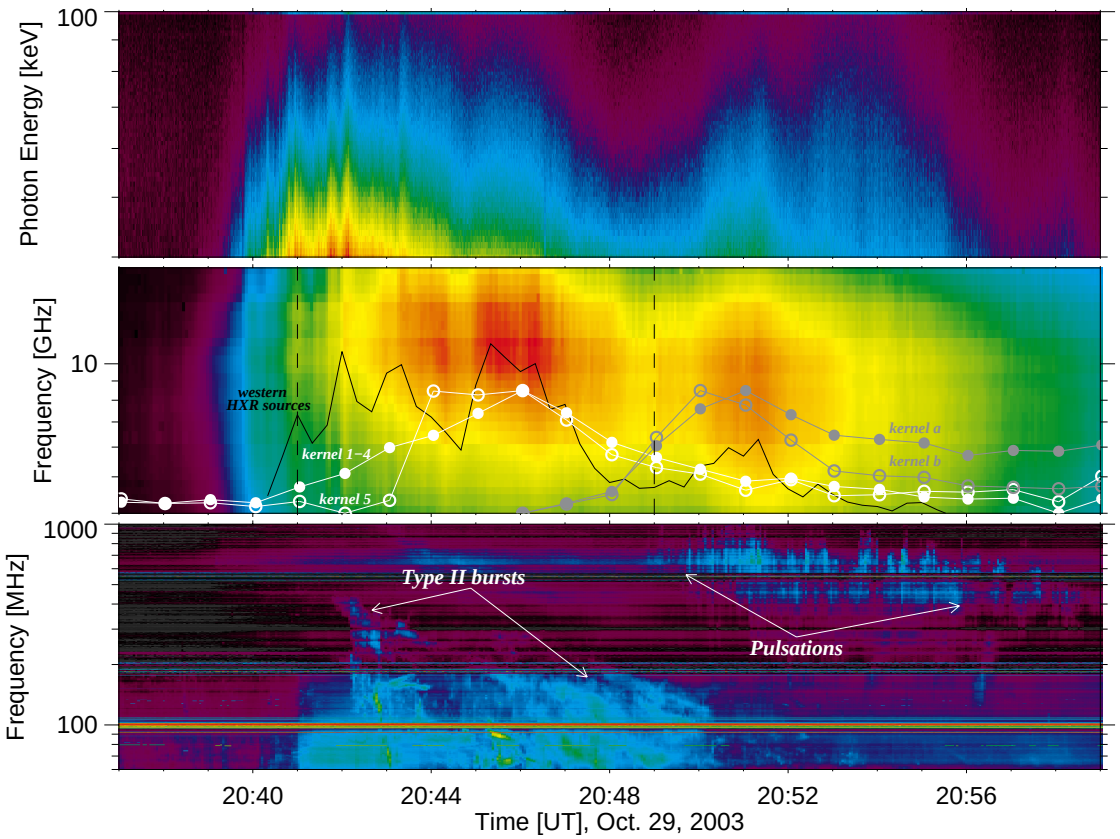

Fig. 9.— Dynamic spectra in *RHESSI* hard X-ray (*top panel*), OVSA microwave (*middle panel*), and Culgoora radio (*bottom panel*) wavelengths. Overplotted in the middle panel, the filled/unfilled white and gray circles represent the time evolutions of intensity of the major remote brightening patches in the eastern site (kernels 1-4/5 in Fig. 2) and southern site (kernels a/b in Fig. 3), respectively. The black line is the lightcurve of western hard X-ray sources shown in Fig. 11. The vertical dashed lines indicate the onset times of the eastern remote brightening kernels 1-4 (at 20:41 UT) and the southern remote brightening kernels (at 20:49 UT).

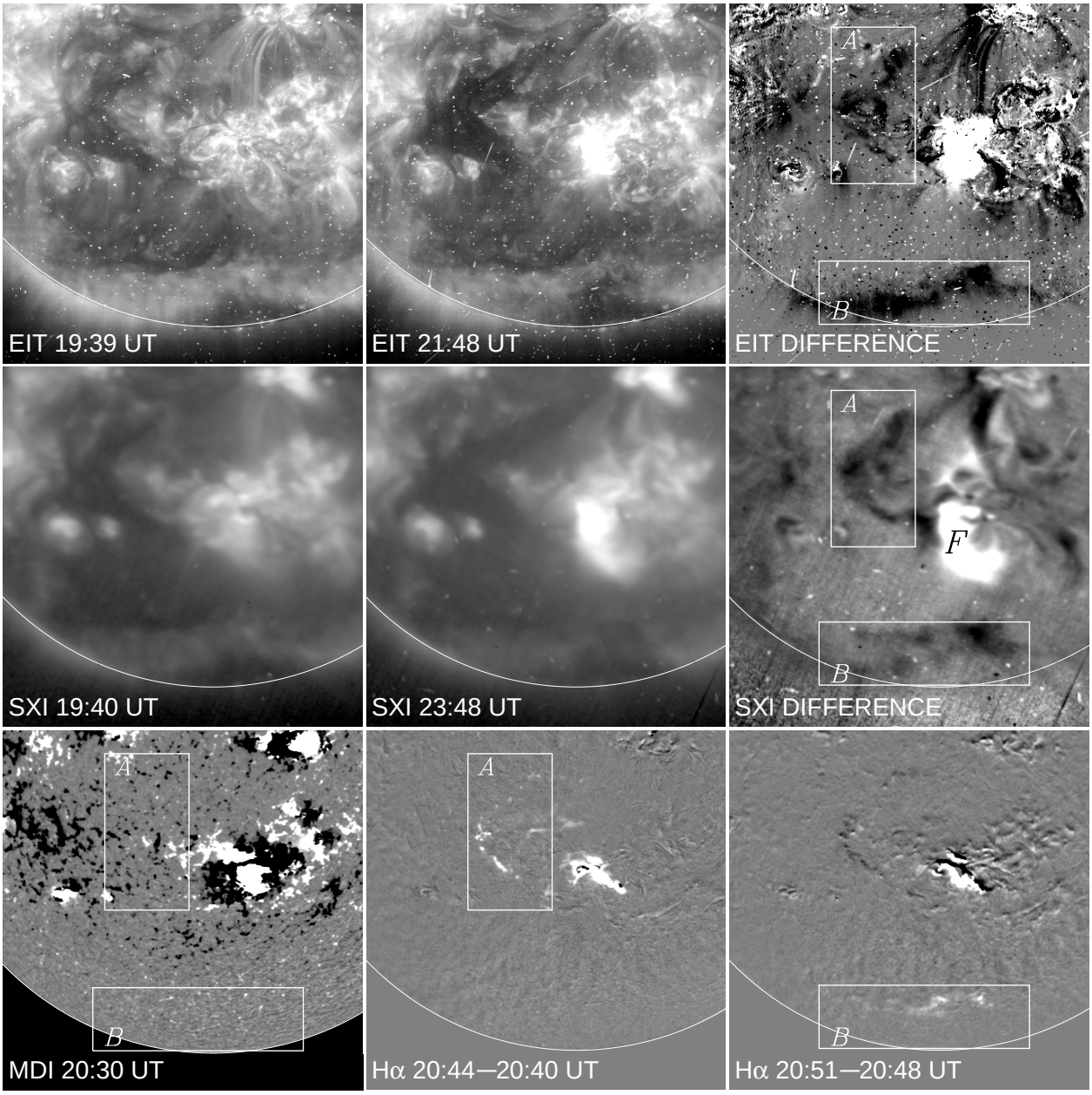

Fig. 10.— *Top row*: pre- and postflare EIT 195 Å images and the difference, showing the EUV dimming associated with the 2003 October 29 flare/CME. Two dimming regions are outlined by boxes *A* and *B*. *Middle row*: pre- and postflare *SXI* soft X-ray images and the difference, showing the similar dimming regions as EUV. "F" denotes the flare core region. *Bottom row*: MDI magnetogram (*left*), Hα difference image showing the eastern remote brightening (*middle*), and Hα difference image showing the southern remote brightening (*right*). The field of view is $1200'' \times 1200''$.

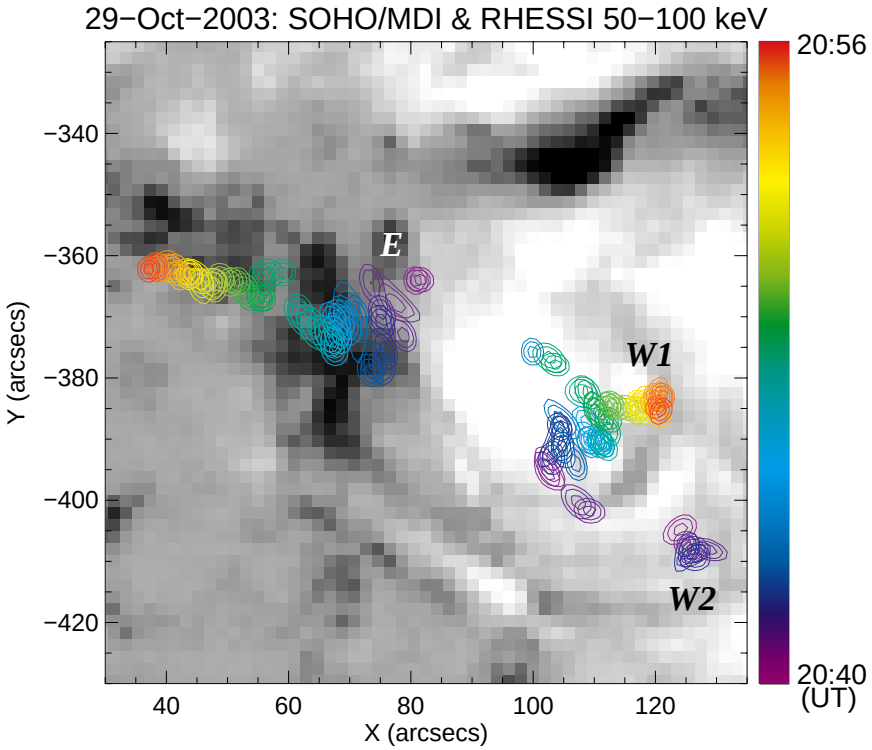

Fig. 11.— Temporal evolution of 50–100 keV hard X-ray source is superposed onto a MDI magnetogram (20:50 UT). Each cleaned *RHESSI* image is integrated over 20 seconds (5 spacecraft spin periods) with 9.4″ FWHM resolution (using grids 3 to 7). Contour levels are 90%, 94%, and 98% of the maximum counts of each source illustrating its centroid position. The changing color of the contours represents times from 20:40:30 to 20:56:10 UT. The eastern (E) and western (W1) sources show clear separation motion after about 20:49 UT.

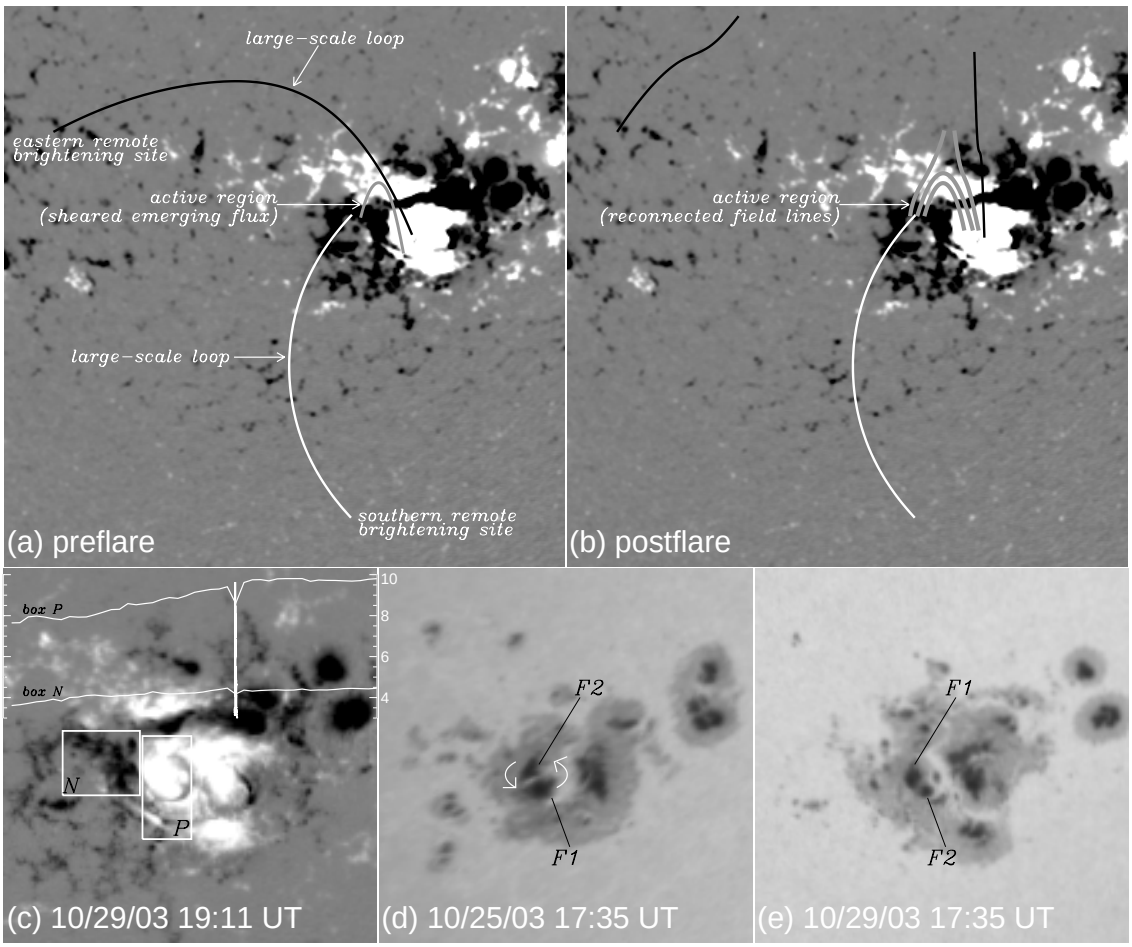

Fig. 12.— Schematic picture showing the preflare (*a*) and postflare (*b*) magnetic configuration. See text for detailed explanation. (*c*) Preflare magnetogram obtained by MDI, superposed with the 3-day time profiles from October 28 00 UT of the measured absolute magnetic flux within the positive and negative polarity region P and N (as denoted by the boxes), respectively, where the October 29 X10 flare (denoted by the curve of vertical spike that represents the lightcurve of *RHESSI* 50–100 keV photons) occurred. The values for the Y-axis give the magnetic flux in 10^{21} Mx. (*d,e*) MDI white-light intensitygrams showing the rotational motion of spots F1 and F2 during about 4 days period before the flare. The field of view of (*a,b*) and (*c–e*) is $780''\times 780''$ and $290''\times 290''$, respectively.